Analysis and modeling of combination bands of sulfur hexafluoride 32 SF 6 based on global fits. Update of the SHeCaSDa database

H. Ke, V. Boudon, Cyril Richard, V. Madhur, M. Faye, L. Manceron

Analysis and modeling of combination bands of sulfur hexafluoride $^{32}SF_6$ based on global fits. Update of the SHeCaSDa database.

H. Ke[a], V. Boudon[a], C. Richard[a], V. Madhur[a], M. Faye[b], L. Manceron[b,c]

[a] *Laboratoire Interdisciplinaire Carnot de Bourgogne, UMR 6303 CNRS / Université Bourgogne Franhce-Comté, 9 Av. A. Savary, BP 47870, F-201078 Dijon Cedex, France*
[b] *Synchrotron SOLEIL, AILES Beamline, L'Orme des Merisiers, St-Aubin BP48, 91192 Cedex, France*
[c] *MONARIS, UMR 8233, CNRS-Sorbonne Université, 4 Place Jussieu, case 49, F-75252 Paris Cedex 05, France*

Abstract

Sulfur hexafluoride is a powerful greenhouse gas of industrial origin. Remote-sensing detection of this heavy species requires a detailed knowledge of its infrared absorption spectra that features many hot bands at room temperature. It is thus necessary to study many of its rovibrational levels which are implied in such hot band transitions. Based on our previous results reporting global fits of many rovibrational bands [M. Faye *at al.*, J. Quant. Spectrosc. Radiat. Transfer **190**, 38–47 (2017)], we present here detailed analyses of three combination bands, namely $\nu_1 + \nu_4$, $\nu_2 + \nu_6$ and $\nu_5 + \nu_6$. The $\nu_2 + \nu_6$ combination band has been already investigated some years ago, but the present analysis represents a strong improvement; the two other bands are analyzed in detail for the first time. The results contribute to improve the simulation of hot bands in the strongly absorbing ν_3 and ν_4 regions and they have been used to update the SHeCaSDa database (`http://vamdc.icb.cnrs.fr/PHP/shecasda.php`).

Keywords: Sulfur hexafluoride, Greenhouse gases, Combination bands, Tensorial formalism, Spectroscopic database update

1. Introduction

Sulfur hexafluoride (SF_6) is a very strong greenhouse gas of industrial origin and whose concentration should be monitored and reduced, according to the Kyoto Protocol [1, 2, 3, 4, 5, 6, 7, 8]. It has a very long lifetime in the atmosphere of around 3200 years [9], since it is chemically inert. It is also used as an atmospheric tracer [10, 11, 12, 13, 14]. In order to perform remote-sensing detection of this molecule, one needs a very good modeling and/or a complete rovibrational line database for is infrared absorption spectrum. This is, however, quite difficult for SF_6. This heavy species possesses a dense and complex spectrum. Due to the presence of low-lying vibrational states, the ground state population is only 32 % at room temperature [15] and, as a consequence, a large number of hot band transitions constitutes the major part the absorption spectrum of SF_6. At present, public databases HITRAN [16] and GEISA [17] are largely incomplete for this molecule: they only contain ν_4 and ν_3 cold band lines and $\nu_4 + \nu_6 - \nu_6$ hot band lines for the main isotopologue, $^{32}SF_6$, as calculated from our previous works and given a supplementary files.

In order to compute hot band spectra, one needs to get a detailed knowledge of the different rovibrational levels implied in these transitions. For this, for many years, we have undertaken a systematic study of as many as possible vibrational bands [15]. As a matter of fact, despite some early pioneering works using simplified models [18, 19, 20], no detailed systematic and quantitative study existed before the very end of the 1990's. Our first work was dedicated to the first analysis of a combination band of SF_6, namely $\nu_2 + \nu_6$, using supersonic jet-cooled infrared absorption spectroscopy [21]. Then, high-resolution stimulated Raman spectroscopy from the CSIC group in Madrid was of great importance to access vibrational levels with g parity of this centrosymmetric species [22, 23, 24, 25]. The ν_4 bending region in the infrared could be studied, along with the first hot band to be analyzed for this species, namely $\nu_4 + \nu_6 - \nu_6$ [26]. Different combination and difference bands could also be analyzed [27, 28, 29, 30]. The low-lying "forbidden" mode ν_6, which is the origin

of many hot bands, could be studied in detail for the first time, since it gains a very weak intensity through Coriolis couplings with other vibrational modes [31]. Finally, we recently published a detailed study of many stretching bands using global fits [32].

Some works were also dedicated to SF_6's minor isotopologues $^{33}SF_6$ [21], $^{34}SF_6$ [21, 24, 25] and even $^{36}SF_6$ [33].

All these studies were carried out thanks to the tensorial formalism tools developed in the Dijon group [34, 35, 36, 37, 38] and to the XTDS and SPVIEW dedicated softwares [39].

Relying on the results of our recent global fits [32], we present in this paper new analyses of three combination bands of $^{32}SF_6$, namely $\nu_1 + \nu_4$, $\nu_2 + \nu_6$ (as a strong improvement compared to Refs. [21, 22]) and $\nu_3 + \nu_5$. This continues the "SF_6 combination level quest".

Section 2 presents some general considerations about the theoretical model and tools used. We present the experimental details in Section 3, while Section 4 gives the analysis, assignment and simulation results. Section 5 explains the recent update of the SheCaSDa (**S**ulfur **He**xafluoride **C**alculated **S**pectroscopic **Da**tabase) database of SF_6 calculated line lists that is built in the framework of the VAMDC international portal [40, 41, 42, 43]. Finally, Section 6 concludes and gives some perspectives to this work.

2. Theoretical elements

2.1. Generalities about SF_6 vibrations

In its equilibrium configuration, SF_6 is a centrosymmetric regular octahedron, belonging to the O_h point group. The SF_6 molecule has six normal vibrational modes [15]:

- ν_1 is a non-degenerate stretching mode with A_{1g} symmetry (band center: 774.5 cm^{-1});
- ν_2 is a doubly degenerate stretching mode with E_g symmetry (band center: 643.4 cm^{-1});

- ν_3 is a triply degenerate stretching mode with F_{1u} symmetry (band center: 948.1 cm^{-1});
- ν_4 is a triply degenerate bending mode with F_{1u} symmetry (band center: 615.0 cm^{-1});
- ν_5 is a triply degenerate bending mode with F_{2g} symmetry (band center: 523.5 cm^{-1});
- ν_6 is a triply degenerate bending mode with F_{2u} symmetry (band center: 346.9 cm^{-1}).

Among those vibrations, only the F_{1u} fundamental vibrational modes (ν_3 and ν_4) are IR active, while A_{1g}, E_g and F_{2g} vibrational modes (ν_1, ν_2 and ν_5) are Raman scattering active only, in first approximation. The F_{2u} fundamental (ν_6) is inactive in both IR absorption and Raman scatting, again in first approximation, although it can get a faint intensity through Coriolis couplings with the other modes [31].

Following group theoretical symmetry rules, harmonic and combination bands of the above-described normal modes usually possess several vibrational sublevels, which are separated through anharmonic interactions. For instance, the three combination bands studied in this article have the following sublevels:

- Combination band $\nu_1 + \nu_4$ contains olny one sublevel, since

$$A_{1g} \otimes F_{1u} = F_{1u}. \tag{1}$$

- Combination band $\nu_2 + \nu_6$ contains two sublevels, since

$$E_g \otimes F_{2u} = F_{1u} \oplus F_{2u}. \tag{2}$$

- Combination band $\nu_5 + \nu_6$ contains four sublevels, since

$$F_{2g} \otimes F_{2u} = A_{1u} \oplus E_u \oplus F_{1u} \oplus F_{2u}. \tag{3}$$

(in the above expressions, $\otimes$ represents the direct product and $\oplus$ the direct sum of O_h group irreducible representations).

Vibrational transitions follow the parity selection rule: since the dipole moment operator has u parity, dipolar absorption or emission imply a parity change ($u \to g$ or $g \to u$) between the initial and final vibrational state, while a Raman scatttering transition implying the polarizability operator with g parity implies parity conservation ($g \to g$ or $u \to u$). The IR absorption active vibrational bands have thus u parity and the Raman scattering active vibrational bands have g parity. In other words, when starting from the ground state (g parity), one can only reach u parity vibrational levels trough IR absorption, or g parity vibrational levels by using Raman spectroscopy. The sublevels of $\nu_1+\nu_4$, $\nu_2+\nu_6$ and $\nu_5+\nu_6$ have u parity, and are thus observable through IR absorption. Since SF_6 is a heavy molecule with low-lying vibrational levels that are heavily populated at room temperature, however, it is necessary to cool down the molecules in order to simplify the spectrum by removing as many as possible of these hot band transitions.

2.2. Effective Hamiltonian

We use here the tensorial formalism and vibrational extrapolation methods developed in the Dijon group [34, 35, 36] and that were specially adapted to octahedral molecules in Ref. [37]. This formalism is implemented in the XDTS software [39]. We summarize here the essential points which are important for the present study.

We can construct the rovibrational Hamiltonian for the SF_6 molecule in the following manner. The rovibrational Hamiltonian operator for a given group of vibrational levels, of polyad, say P_k (see below), is expanded in the form:

$$H_{\{P_k\}} = \sum_{\text{all indices}} t^{\Omega(K,n\Gamma)\Gamma_v\Gamma'_v}_{\{s\}\{s'\}} T^{\Omega(K,n\Gamma)\Gamma_v\Gamma'_v}_{\{s\}\{s'\}}. \tag{4}$$

In this equation, all indices stand for intermediate quantum numbers and symmetries. Briefly, Γ, Γ_v and Γ'_v are a rotational and two vibrational irreducible representations, respectively, while K is an integer (rotational degree), n is a multiplicity index (counting identical irreducible representations Γ for a given

K value), while $\{s\}$ and $\{s'\}$ represent intermediate symmetry labels in the construction of vibrational operators [34]; Ω is defined below. The term $t^{\Omega(K,n\Gamma)\Gamma_v\Gamma'_v}_{\{s\}\{s'\})}$ represents numerical parameters of the model to be fitted using experimental line assignments. The term $T^{\Omega(K,n\Gamma)\Gamma_v\Gamma'_v}_{\{s\}\{s'\}}$ refers to totally symmetric rovibrational operators:

$$T^{\Omega(K,n\Gamma)\Gamma_v\Gamma'_v}_{\{s\}\{s'\}} = \beta(R^{\Omega(K,n\Gamma)} \otimes {}^{\varepsilon}V^{\Gamma_v\Gamma'_v(\Gamma)}_{\{s\}\{s'\}})^{(A_{1g})}, \tag{5}$$

where β is a numerical factor used to modify the scalar terms so that they get a standard form:

$$\beta = \begin{cases} \sqrt{[\Gamma]}(-\sqrt{3}/4)^{\Omega/2} & , \text{ if}(K, n\Gamma) = (0, 0A_{1g}), \\ 1 & , \text{ otherwise}, \end{cases} \tag{6}$$

where $[\Gamma]$ is the dimension of irreducible representation Γ. $R^{\Omega(K,n\Gamma)}$ is a rotational operator of degree Ω in the angular momentum components (J_x, J_y, J_z), while ${}^{\varepsilon}V^{\Gamma_v\Gamma'_v(\Gamma)}_{\{s\}\{s'\}}$ is a vibrational operator of degree Ω_v in vibration creation and annihilation operators. The order of each individual term is defined as $\Omega + \Omega_v - 2$. The recursive construction of these operators has been described elsewhere [44, 34, 36].

Consider a species whose molecular vibrational levels are grouped into a series of polyads named P_k $(k = 0, ..., n)$, P_0 being the ground state. We can expand the rovibrational effective Hamiltonian operator as follows, after performing some Van Vleck [45] contact transformations to isolate polyads [34]:

$$\widetilde{H} = H_{\{P_0\}} + H_{\{P_1\}} + ... + H_{\{P_n\}}, \tag{7}$$

where $H_{\{P_k\}}$ contains rovibrational operators with no matrix element within the $P_{k'<k}$ basis sets. The effective Hamiltonian for polyad P_n is obtained by projecting H in the P_n Hilbert subspace:

$$\widetilde{H}^{<P_n>} = P^{<P_n>} H P^{<P_n>} = H^{<P_n>}_{\{GS\}} + ... + H^{<P_n>}_{\{P_k\}} + ... + H^{<P_n>}_{\{P_n\}}. \tag{8}$$

2.3. SF_6 polyad schemes

The SF_6 molecule has a quite complex vibrational level distribution, with no clear polyad structure, the six fundamental vibrational wavenumbers being ran-

domly distributed without simple ratios between them. It is possible, however, to define some partial polyad schemes in order to treat together several levels showing specific interactions. This was done in our previous work about excited states of this molecule [32]. In particular, we used in this paper a scheme allowing a global fit of lines from 12 rovibrational bands, giving fitted parameters for 10 different stretching vibrational levels. Figure 10 in the Appendix illustrates this polyad scheme. It was then possible to reconsider the ν_6 "forbidden band" [31] together with the ν_4 and $\nu_4 + \nu_6 - \nu_6$ bands [26] altogether using a second polyad scheme, as described in Figure 11 in the Appendix. Schemes number 3 and 4 are also used for levels implying bending modes, as in Ref. [46] and [30], see Figure 12 in the Appendix.

At each step, the parameters determined in previous fits are fixed, as indicated in Figures 10 to 13 in the Appendix. Results of these global fits can be found in Table 5 of Ref. [32] and Table 2 of Ref. [46]. Using all these results to get reliable effective Hamiltonian parameters for the Ground State, ν_1, ν_4, ν_5 and ν_6, levels it was then possible to define new simple polyad schemes (see Figure 13 in the Appendix) in order to assign and fit three additional combination bands, namely $\nu_1 + \nu_4$, $\nu_2 + \nu_6$ and $\nu_5 + \nu_6$. It should be again noticed that $\nu_2 + \nu_6$ has been studied previously [21, 22], but that the new spectra used in the present work allowed a very strong improvement, as we detail it below. We thus only detailed here the effective Hamiltonians used for the study of these three bands, that are:

- The ground state effective Hamiltonian,

$$H^{<GS>} = H^{<GS>}_{\{GS\}}. \tag{9}$$

- The ν_i $(i = 1, 2, 4, 5, 6)$ fundamental band effective Hamiltonians,

$$H^{<\nu_i>} = H^{<\nu_i>}_{\{GS\}} + H^{<\nu_i>}_{\{\nu_i\}}. \tag{10}$$

- The $\nu_1 + \nu_4$ combination level effective Hamiltonian,

$$H^{<\nu_1+\nu_4>} = H^{<\nu_1+\nu_4>}_{\{GS\}} + H^{<\nu_1+\nu_4>}_{\{\nu_4\}} + H^{<\nu_1+\nu_4>}_{\{\nu_1\}} + H^{<\nu_1+\nu_4>}_{\{\nu_1+\nu_4\}}. \tag{11}$$

- The $\nu_2 + \nu_6$ combination level effective Hamiltonian,

$$H^{<\nu_2+\nu_6>} = H^{<\nu_2+\nu_6>}_{\{GS\}} + H^{<\nu_2+\nu_6>}_{\{\nu_6\}} + H^{<\nu_2+\nu_6>}_{\{\nu_2\}} + H^{<\nu_2+\nu_6>}_{\{\nu_2+\nu_6\}}. \quad (12)$$

- The $\nu_5 + \nu_6$ combination level effective Hamiltonian,

$$H^{<\nu_5+\nu_6>} = H^{<\nu_5+\nu_6>}_{\{GS\}} + H^{<\nu_5+\nu_6>}_{\{\nu_6\}} + H^{<\nu_5+\nu_6>}_{\{\nu_5\}} + H^{<\nu_5+\nu_6>}_{\{\nu_5+\nu_6\}}. \quad (13)$$

2.4. Basis sets

To calculate line positions and strengths, we use a coupled vibrational basis set taking into account the different vibrational modes of XY_6 molecules. The Hamiltonian and dipole moment matrix elements are then calculated in the coupled rovibrational basis set with symmetry C (O_h group irreducible representation):

$$\left|(\Psi_r^{(J,nC_r)} \otimes \Psi_v^{C_v})^{(C)}\right\rangle, \quad (14)$$

where $\Psi_r^{(J,nC_r)}$ is a rotational wavefunction with symmetry C_r (n being a multiplicity index to distinguish identical representations C for a given rotational quantum number value J) and $\Psi_v^{(C_v)}$ is a vibrational wavefunction with symmetry C_v. The latter ones are constructed [37, 36] by coupling harmonic oscillator basis sets:

- The ν_1 vibrational functions are all totally symmetric,

$$\left|\Psi_{v_1}^{(A_{1g})}\right\rangle. \quad (15)$$

- The doubly degenerate mode basis set is

$$\left|\Psi_{v_2}^{(l_2,C_2)}\right\rangle, \quad (16)$$

where $l_2 = v_2, v_2 - 2, ..., -v_2$.

- The vibrational basis set for the triply degenerate modes is written as

$$\left|\Psi_v^{(l,n_vC_n)}\right\rangle, \quad (17)$$

where n_v is a multiplicity index (counting identical representations C_n for a given l value) and the quantum number is $l = v, v - 2, ..., 0$ *or* 1.

2.5. Line intensities

In order to calculate line intensities for dipolar absorption transitions, the dipole moment operator is expanded using the same tensorial formalism. Its construction has been described previously for octahedral XY_6 molecules [37, 47, 36]. Since in the present study we only consider relative intensities for the rovibrational lines of the three combination bands under investigation, the dipole moment was only expanded to a low order. It includes a first-order term (main dipole moment derivative) and a second order term (Herman-Wallis term) used to "equilibrate" the P and R branch intensities when performing synthetic spectrum simulations. Thus, we do not detail more the dipole moment formalism here.

3. Experimental setup

The experimental high resolution spectra were recorded at the AILES Beamline at Synchrotron SOLEIL on the Synchrotron light source[48, 49] by Mbaye Faye during his PhD thesis [50]. The line is coupled to the Bruker 125HR interferometer and uses a cryogenic multipass cell set on a 15 m optical path length and regulated at 153 ± 2 K temperature along the entire optical path. This setup is fully described in Ref. [51]. The cell optical set-up is based on a 1.5 m base length Barskaya-Chernin five-mirrors arrangement[52].

The cell is mounted inside a triple jacket-liquid nitrogen cryostat. The cooling power from a liquid nitrogen-filled surrounding envelope is transmitted by an annular space filled by helium as convection gas, whose pressure can be varied to adjust the cooling power. Additional heaters are distributed along the gas cell body for temperature homogenization. The cell and the outside Dewar jacket are fitted with diamond windows brazed on stainless steel flanges to enable operation of the cell between 80 K and 400 K from the near IR to the THz range. A spectrum with a gas pressure of 0.09 mbar of SF_6 (Air Liquide, France, 99.9% purity) was recorded at 0.0025 cm^{-1} resolution in the $700 - 2000$ cm^{-1} region with no apodization, 5.06 cm/s mirror velocity, a Ge/KBr beamsplitter

and a HgCdTe detector. 1426 interferograms were averaged in a total recording time of about 38 hours and processed against a background of the empty cell taken at the same 153 K temperature at 0.01 cm^{-1} resolution. Spectra were zero-filled, corrected for channelling effects and calibrated using well-known water rotational lines [53, 54]. The frequency accuracy is here 3×10^{-4} cm^{-1} (one sigma).

4. Analysis of simulation results

Thanks to the XTDS and SPVIEW softwares [39] developed in the Dijon group that implement the above-described formalism (XTDS) and that allow on-screen line assignments (SPVIEW), the simulation and analysis of combination bands $\nu_1 + \nu_4$, $\nu_2 + \nu_6$ and $\nu_5 + \nu_6$ is a relatively easy.

First of all, we calculate in each case an approximate spectrum with pre-existing parameters taken from previous works for the lower levels (GS, ν_1, ν_2, ν_5 and ν_6). In this first step, anharmonicity parameters for the combination bands are fixed by hand in order to match the correct band center, as detailed for instance in Section 4.1. Next, we assign the simulated absorption peaks to the experimental spectrum by using the SPVIEW software (this one allows to assign experimental lines to calculated transitions by comparing the two spectra and by clicking on the lines). After that, the effective Hamiltonian parameters are fitted thanks to a non-linear least-squares fit method (Levenberg-Marquardt algorithm). To correct the simulated spectrum, and assign more lines, these steps were repeated several times until a good simulation spectrum is obtained and considered as perfectly similar to the experimental spectrum (with no further assignment being possible and a root-mean-square deviation of a few 10^{-4} cm^{-1} for the fit of the effective Hamiltonian parameters). Table 1 gives the effective Hamiltonian parameters we obtain. Please refer to Table 5 of Ref. [32] and Table 2 of Ref. [46] for lower state parameters. The following paragraphs give more detailed explanations for the three different combination bands under study.

Table 1: Fitted effective Hamiltonian parameters for the $\nu_1+\nu_4$, $\nu_2+\nu_6$ and $\nu_5+\nu_6$ combination bands. Lower-state parameters are fixed from previous global fits (see text).

Band	Parameter (notations of Section 2.2)			Value / cm^{-1}	Comments
	$\Omega(K,n\Gamma)$	$(s)\Gamma_v$	$(s')\Gamma'_v$		
$\nu_1+\nu_4$	$0(0,0A_{1g})$	$100100F_{1u}$	$100100F_{1u}$	$-1.145635(56)$	Anhrmonicity X_{14}
	$1(1,0F_{1g})$	$100100F_{1u}$	$100100F_{1u}$	$-5.358(39)\times10^{-4}$	Coriolis interaction
	$2(0,0A_{1g})$	$100100F_{1u}$	$100100F_{1u}$	$-9.2(2.1)\times10^{-8}$	ΔB_{14}
	$2(2,0E_g)$	$100100F_{1u}$	$100100F_{1u}$	$0.0^\dagger$	
	$2(2,0F_{2g})$	$100100F_{1u}$	$100100F_{1u}$	$0.0^\dagger$	
	$3(1,0F_{1g})$	$100100F_{1u}$	$100100F_{1u}$	$-5.14(48)\times10^{-9}$	
	$3(3,0F_{1g})$	$100100F_{1u}$	$100100F_{1u}$	$-3.22(25)\times10^{-9}$	
$\nu_2+\nu_6$	$0(0,0A_{1g})$	$010001F_{1u}$	$010001F_{1u}$	$1.64179(77)\times10^{-1}$	F_{1u} sublevel
	$1(1,0F_{1g})$	$010001F_{1u}$	$010001F_{1u}$	$-1.3065(63)\times10^{-3}$	Coriolis interaction
	$2(0,0A_{1g})$	$010001F_{1u}$	$010001F_{1u}$	$-5.269(56)\times10^{-5}$	
	$2(2,0E_g)$	$010001F_{1u}$	$010001F_{1u}$	$-3.779(41)\times10^{-5}$	
	$2(2,0F_{2g})$	$010001F_{1u}$	$010001F_{1u}$	$8.169(65)\times10^{-5}$	
	$3(1,0F_{1g})$	$010001F_{1u}$	$010001F_{1u}$	$1.052(18)\times10^{-7}$	
	$3(3,0F_{1g})$	$010001F_{1u}$	$010001F_{1u}$	$5.28(18)\times10^{-8}$	
	$4(0,0A_{1g})$	$010001F_{1u}$	$010001F_{1u}$	$-1.44(28)\times10^{-10}$	
	$4(2,0E_g)$	$010001F_{1u}$	$010001F_{1u}$	$-2.6(1.4)\times10^{-11}$	
	$4(2,0F_{2g})$	$010001F_{1u}$	$010001F_{1u}$	$-3.10(26)\times10^{-10}$	
	$4(4,0A_{1g})$	$010001F_{1u}$	$010001F_{1u}$	$2.37(63)\times10^{-11}$	
	$4(4,0E_g)$	$010001F_{1u}$	$010001F_{1u}$	$9.9(1.1)\times10^{-11}$	
	$4(4,0F_{2g})$	$010001F_{1u}$	$010001F_{1u}$	$0.0^\dagger$	
	$1(1,0F_{1g})$	$010001F_{1u}$	$010001F_{2u}$	$7.261(19)\times10^{-3}$	$F_{1u}-F_{2u}$ interaction
	$2(2,0E_g)$	$010001F_{1u}$	$010001F_{2u}$	$4.196(40)\times10^{-5}$	
	$2(2,0F_{2g})$	$010001F_{1u}$	$010001F_{2u}$	$2.725(77)\times10^{-6}$	
	$3(1,0F_{1g})$	$010001F_{1u}$	$010001F_{2u}$	$0.0^\dagger$	
	$3(3,0A_{2g})$	$010001F_{1u}$	$010001F_{2u}$	$0.0^\dagger$	
	$3(3,0F_{1g})$	$010001F_{1u}$	$010001F_{2u}$	$0.0^\dagger$	
	$3(3,0F_{2g})$	$010001F_{1u}$	$010001F_{2u}$	$0.0^\dagger$	
	$0(0,0A_{1g})$	$010001F_{2u}$	$010001F_{2u}$	$-1.92162(13)$	F_{2u} sublevel
	$1(1,0F_{1g})$	$010001F_{2u}$	$010001F_{2u}$	$3.8380(76)\times10^{-3}$	Coriolis interaction
	$2(0,0A_{1g})$	$010001F_{2u}$	$010001F_{2u}$	$4.243(57)\times10^{-5}$	
	$2(2,0E_g)$	$010001F_{2u}$	$010001F_{2u}$	$2.960(43)\times10^{-5}$	
	$2(2,0F_{2g})$	$010001F_{2u}$	$010001F_{2u}$	$-5.932(63)\times10^{-5}$	
	$3(1,0F_{1g})$	$010001F_{2u}$	$010001F_{2u}$	$-9.26(16)\times10^{-8}$	
	$3(3,0F_{1g})$	$010001F_{2u}$	$010001F_{2u}$	$-7.08(14)\times10^{-8}$	
	$4(0,0A_{1g})$	$010001F_{2u}$	$010001F_{2u}$	$0.0^\dagger$	
	$4(2,0E_g)$	$010001F_{2u}$	$010001F_{2u}$	$0.0^\dagger$	
	$4(2,0F_{2g})$	$010001F_{2u}$	$010001F_{2u}$	$0.0^\dagger$	
$\nu_5+\nu_6$	$0(0,0A_{1g})$	$000011A_{1u}$	$000011A_{1u}$	$-1.389(79)\times10^{-1}$	A_{1u} sublevel

† Fixed value.

Continued from Table 1.

Band	Parameter (notations of Section 2.2)			Value / cm^{-1}	Comments
	$\Omega(K, n\Gamma)$	$(s)\Gamma_v$	$(s')\Gamma'_v$		
	$2(0,0A_{1g})$	$000011A_{1u}$	$000011A_{1u}$	$0.0^{\dagger}$	
	$4(0,0A_{1g})$	$000011A_{1u}$	$000011A_{1u}$	$0.0^{\dagger}$	
	$4(4,0A_{1g})$	$000011A_{1u}$	$000011A_{1u}$	$0.0^{\dagger}$	
	$2(2,0E_g)$	$000011A_{1u}$	$000011E_u$	$-1.10(21) \times 10^{-4}$	$A_{1u} - E_u$ interaction
	$4(2,0E_g)$	$000011A_{1u}$	$000011E_u$	$-3.36(33) \times 10^{-8}$	
	$4(4,0E_g)$	$000011A_{1u}$	$000011E_u$	$0.0^{\dagger}$	
	$1(1,0F_{1g})$	$000011A_{1u}$	$000011F_{1u}$	$0.0^{\dagger}$	
	$3(1,0F_{1g})$	$000011A_{1u}$	$000011F_{1u}$	$0.0^{\dagger}$	
	$3(3,0F_{1g})$	$000011A_{1u}$	$000011F_{1u}$	$0.0^{\dagger}$	
	$4(4,0F_{1g})$	$000011A_{1u}$	$000011F_{1u}$	$0.0^{\dagger}$	
	$2(2,0F_{2g})$	$000011A_{1u}$	$000011F_{2u}$	$3.58(35) \times 10^{-4}$	$A_{1u} - F_{2u}$ interaction
	$3(3,0F_{2g})$	$000011A_{1u}$	$000011F_{2u}$	$2.52(21) \times 10^{-6}$	
	$4(2,0F_{2g})$	$000011A_{1u}$	$000011F_{2u}$	$-2.88(37) \times 10^{-8}$	
	$4(4,0F_{2g})$	$000011A_{1u}$	$000011F_{2u}$	$1.71(25) \times 10^{-8}$	
	$0(0,0A_{1g})$	$000011E_u$	$000011E_u$	$-3.901(53) \times 10^{-1}$	E_u sublevel
	$2(0,0A_{1g})$	$000011E_u$	$000011E_u$	$0.0^{\dagger}$	
	$2(2,0E_g)$	$000011E_u$	$000011E_u$	$0.0^{\dagger}$	
	$3(3,0A_{2g})$	$000011E_u$	$000011E_u$	$0.0^{\dagger}$	
	$4(0,0A_{1g})$	$000011E_u$	$000011E_u$	$0.0^{\dagger}$	
	$4(2,0E_g)$	$000011E_u$	$000011E_u$	$0.0^{\dagger}$	
	$4(4,4A_{1g})$	$000011E_u$	$000011E_u$	$0.0^{\dagger}$	
	$4(4,0E_g)$	$000011E_u$	$000011E_u$	$0.0^{\dagger}$	
	$1(1,0F_{1g})$	$000011E_u$	$000011F_{1u}$	$-9.25(46) \times 10^{-3}$	$E_u - F_{1u}$ interaction
	$2(2,0F_{2g})$	$000011E_u$	$000011F_{1u}$	$-1.27(11) \times 10^{-4}$	
	$3(1,0F_{1g})$	$000011E_u$	$000011F_{1u}$	$-4.03(42) \times 10^{-7}$	
	$3(3,0F_{1g})$	$000011E_u$	$000011F_{1u}$	$-2.45(42) \times 10^{-7}$	
	$3(3,0F_{2g})$	$000011E_u$	$000011F_{1u}$	$0.0^{\dagger}$	
	$4(2,0F_{2g})$	$000011E_u$	$000011F_{1u}$	$0.0^{\dagger}$	
	$4(4,0F_{1g})$	$000011E_u$	$000011F_{1u}$	$0.0^{\dagger}$	
	$4(4,0F_{2g})$	$000011E_u$	$000011F_{1u}$	$0.0^{\dagger}$	
	$1(1,0F_{1g})$	$000011E_u$	$000011F_{2u}$	$0.0^{\dagger}$	
	$2(2,0F_{2g})$	$000011E_u$	$000011F_{2u}$	$0.0^{\dagger}$	
	$3(1,0F_{1g})$	$000011E_u$	$000011F_{2u}$	$0.0^{\dagger}$	
	$3(3,0F_{1g})$	$000011E_u$	$000011F_{2u}$	$0.0^{\dagger}$	
	$3(3,0F_{2g})$	$000011E_u$	$000011F_{2u}$	$0.0^{\dagger}$	
	$4(2,0F_{2g})$	$000011E_u$	$000011F_{2u}$	$0.0^{\dagger}$	
	$4(4,0F_{1g})$	$000011E_u$	$000011F_{2u}$	$0.0^{\dagger}$	
	$4(4,0F_{2g})$	$000011E_u$	$000011F_{2u}$	$0.0^{\dagger}$	
	$0(0,0A_{1g})$	$000011F_{1u}$	$000011F_{1u}$	$-1.365364(67)$	F_{1u} sublevel
	$1(1,0F_{1g})$	$000011F_{1u}$	$000011F_{1u}$	$4.3826(74) \times 10^{-3}$	Coriolis interaction
	$2(0,0A_{1g})$	$000011F_{1u}$	$000011F_{1u}$	$4.88(20) \times 10^{-5}$	
	$2(2,0E_g)$	$000011F_{1u}$	$000011F_{1u}$	$3.3(1.5) \times 10^{-6}$	

† Fixed value.

Continued from Table 1.

Band	Parameter (notations of Section 2.2)			Value / cm^{-1}	Comments
	$\Omega(K, n\Gamma)$	$(s)\Gamma_v$	$(s')\Gamma'_v$		
	$2(2,0F_{2g})$	$000011F_{1u}$	$000011F_{1u}$	$3.968(99) \times 10^{-5}$	
	$3(1,0F_{1g})$	$000011F_{1u}$	$000011F_{1u}$	$-2.73(29) \times 10^{-7}$	
	$3(3,0F_{1g})$	$000011F_{1u}$	$000011F_{1u}$	$4.73(44) \times 10^{-7}$	
	$4(0,0A_{1g})$	$000011F_{1u}$	$000011F_{1u}$	$0.0^{\dagger}$	
	$4(2,0E_g)$	$000011F_{1u}$	$000011F_{1u}$	$0.0^{\dagger}$	
	$4(2,0F_{2g})$	$000011F_{1u}$	$000011F_{1u}$	$0.0^{\dagger}$	
	$4(4,0A_{1g})$	$000011F_{1u}$	$000011F_{1u}$	$0.0^{\dagger}$	
	$4(4,0E_g)$	$000011F_{1u}$	$000011F_{1u}$	$0.0^{\dagger}$	
	$4(4,0F_{2g})$	$000011F_{1u}$	$000011F_{1u}$	$0.0^{\dagger}$	
	$1(1,0F_{1g})$	$000011F_{1u}$	$000011F_{2u}$	$6.03(55) \times 10^{-3}$	$F_{1u} - F_{2u}$ interaction
	$2(2,0E_g)$	$000011F_{1u}$	$000011F_{2u}$	$-4.38(10) \times 10^{-5}$	
	$2(2,0F_{2g})$	$000011F_{1u}$	$000011F_{2u}$	$2.75(15) \times 10^{-4}$	
	$3(1,0F_{1g})$	$000011F_{1u}$	$000011F_{2u}$	$-2.07(78) \times 10^{-7}$	
	$3(3,0A_{2g})$	$000011F_{1u}$	$000011F_{2u}$	$4.12(31) \times 10^{-7}$	
	$3(3,0F_{1g})$	$000011F_{1u}$	$000011F_{2u}$	$2.38(91) \times 10^{-7}$	
	$3(3,0F_{2g})$	$000011F_{1u}$	$000011F_{2u}$	$0.0^{\dagger}$	
	$4(2,0E_g)$	$000011F_{1u}$	$000011F_{2u}$	$0.0^{\dagger}$	
	$4(2,0F_{2g})$	$000011F_{1u}$	$000011F_{2u}$	$-6.12(26) \times 10^{-9}$	
	$4(4,0E_g)$	$000011F_{1u}$	$000011F_{2u}$	$0.0^{\dagger}$	
	$4(4,0F_{1g})$	$000011F_{1u}$	$000011F_{2u}$	$1.012(65) \times 10^{-8}$	
	$4(4,0F_{2g})$	$000011F_{1u}$	$000011F_{2u}$	$0.0^{\dagger}$	
	$0(0,0A_{1g})$	$000011F_{2u}$	$000011F_{2u}$	$-9.75(48) \times 10^{-2}$	F_{2u} sublevel
	$1(1,0F_{1g})$	$000011F_{2u}$	$000011F_{2u}$	$-9.52(51) \times 10^{-3}$	Coriolis interaction
	$2(0,0A_{1g})$	$000011F_{2u}$	$000011F_{2u}$	$5.36(73) \times 10^{-5}$	
	$2(2,0E_g)$	$000011F_{2u}$	$000011F_{2u}$	$0.0^{\dagger}$	
	$2(2,0F_{2g})$	$000011F_{2u}$	$000011F_{2u}$	$-4.5(1.6) \times 10^{-5}$	
	$3(1,0F_{1g})$	$000011F_{2u}$	$000011F_{2u}$	$5.2(2.0) \times 10^{-7}$	
	$3(3,0F_{1g})$	$000011F_{2u}$	$000011F_{2u}$	$7.9(1.2) \times 10^{-7}$	
	$4(0,0A_{1g})$	$000011F_{2u}$	$000011F_{2u}$	$8.2(1.2) \times 10^{-9}$	
	$4(2,0E_g)$	$000011F_{2u}$	$000011F_{2u}$	$0.0^{\dagger}$	
	$4(2,0F_{2g})$	$000011F_{2u}$	$000011F_{2u}$	$-2.00(16) \times 10^{-8}$	
	$4(4,0A_{1g})$	$000011F_{2u}$	$000011F_{2u}$	$0.0^{\dagger}$	
	$4(4,0E_g)$	$000011F_{2u}$	$000011F_{2u}$	$0.0^{\dagger}$	
	$4(4,0F_{2g})$	$000011F_{2u}$	$000011F_{2u}$	$0.0^{\dagger}$	

† Fixed value.

4.1. The $\nu_1 + \nu_4$ combination band (band center: 1388.382 cm^{-1})

As shown in Figure 1, H_2O molecules were present in the SF_6 sample, resulting in a H_2O line in the P branch of $\nu_1 + \nu_4$ band spectrum. We can see that the P and R branches are well resolved with a quite clear structure. This band being, in first approximation, a simple shift of the well-known ν_4 one [26] (the ν_1 mode being totally symmetric), its assignment starting from ν_4 parameters is quite straightforward. The Q branch is very dense and less resolved but it was possible to assign some lines and reproduce its structure correctly. The simulated spectrum agrees well and ensures the accuracy of the effective Hamiltonian that has been determined. 1322 line positions up to $J = 76$ were assigned and effective Hamiltonian was developed up to order 6 for the ground state, ν_1 and ν_4 vibrational levels and up to order 5 for the $\nu_1 + \nu_4$ level itself. The band center is located at 1388.382 cm^{-1}. Only 5 Hamiltonian parameters were fitted as shown in Table 1. The root-mean-square deviation is 0.456×10^{-3} cm^{-1}. This is the first detailed study and modeling of this band. The parameters obtained here, allow the calculation of the $\nu_4 + \nu_1 - \nu_1$ hot band in the ν_4 region for the SHeCaSDa database (see Section 5).

Figure 2 displays the fit residuals for line positions. Figure 3 displays reduced calculated and observed rovibrational energy levels for this band, after subtraction of scalar terms in the effective Hamiltonian. Observed levels are those reached by assigned transitions. They show the sampling of the energy level spectrum for this level used in the fit.

4.2. The $\nu_2 + \nu_6$ combination band (band center: 991.274 cm^{-1})

As mentioned above, this band has already been studied a long time ago thanks to a cold supersonic molecular jet spectrum [21, 22]. This previous study was a good starting point for the present work. It was then possible to assign here many more lines: 4194 lines up to $J = 78$, instead of 521 lines up to $J = 37$ only.

For this $\nu_2 + \nu_6$ combination band, the spectrum structure is quite complicated and dense as shown in the Figure 4. We should firstly assign several

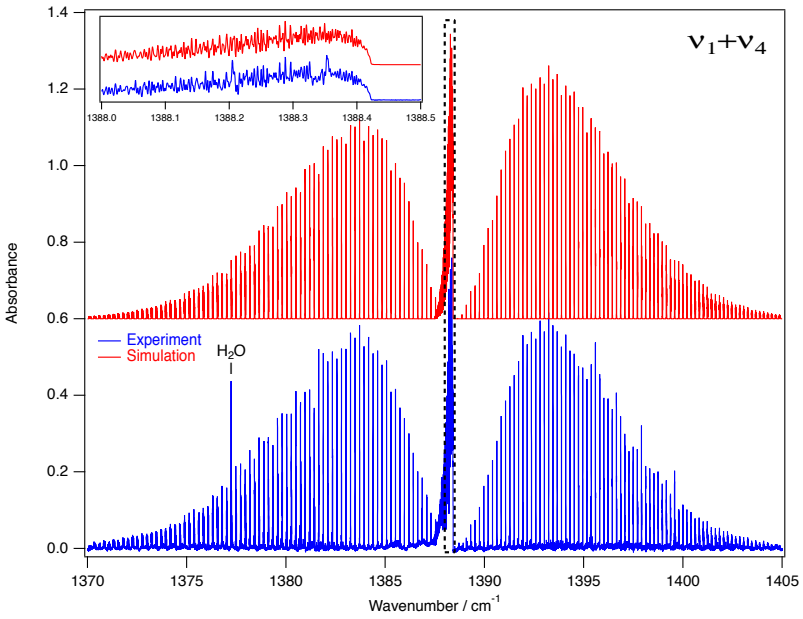

Figure 1: Experimental and simulated spectra for the $\nu_1 + \nu_4$ combination band of SF_6 at 153 K. The insert shows the Q branch. The presence of a H_2O line in the experimental spectrum is indicated.

obvious absorption peaks in both the P and R branch, and then add more absorption peaks, step by step. After repeating the procedure many times, the dense parts were also well simulated. The effective Hamiltonian was developed up to order 6 for the ground state, ν_2, ν_6 and $\nu_2 + \nu_6$ vibrational levels. The F_{1u} and F_{2u} vibrational sublevels are located at 991.274 and 989.119 cm^{-1}, respectively. The F_{1u} sublevel corresponds to the "active" or "allowed" band center (same symmetry as the dipole moment operator) and the strong visible Q branch is centered on it. A total of 22 Hamiltonian parameters were fitted at the same time as shown in Table 1. The root-mean-square deviation is very small: 0.259×10^{-3} cm^{-1} only.

Figure 5 displays the fit residuals for line positions. Figure 6 displays reduced calculated and observed rovibrational energy levels for this band, as in the previous case.

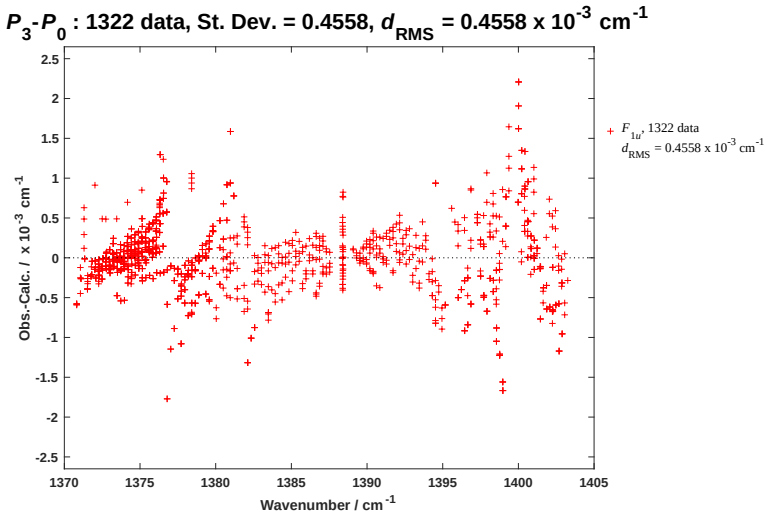

Figure 2: Fit residuals for line positions in the $\nu_1 + \nu_4$ combination band of SF_6.

4.3. The $\nu_5 + \nu_6$ combination band (band center: 870.399 cm^{-1})

As for the $\nu_5 + \nu_6$ combination band, the spectrum structure looks quite simple, although we have here a problem with four sublevels. This indicates that the anharmonic interactions should not split them very much. After assignment and fit, all the peaks were well matched (see Figure 7), even for some peaks with an anomalous intensity in the R branch. We could assign 2992 line positions up to $J = 71$. The effective Hamiltonian was developed up to order 6 for the ground state, ν_5, ν_6 and $\nu_5+\nu_6$ vibrational levels. The "active" F_{1u} band center is located at 870.399 cm^{-1}, while the three others are located around 871.5 cm^{-1}. The positions of these A_{1u}, E_u and F_{2u} should, however, be considered with care. They were obtained through couplings fitted with essentially F_{1u} sublevel assigned peaks. The final result matches remarkably well for the whole band, but the data about these "inactive" levels (or "dark states") many not be very accurate. A total of 35 Hamiltonian parameters were fitted as shown in

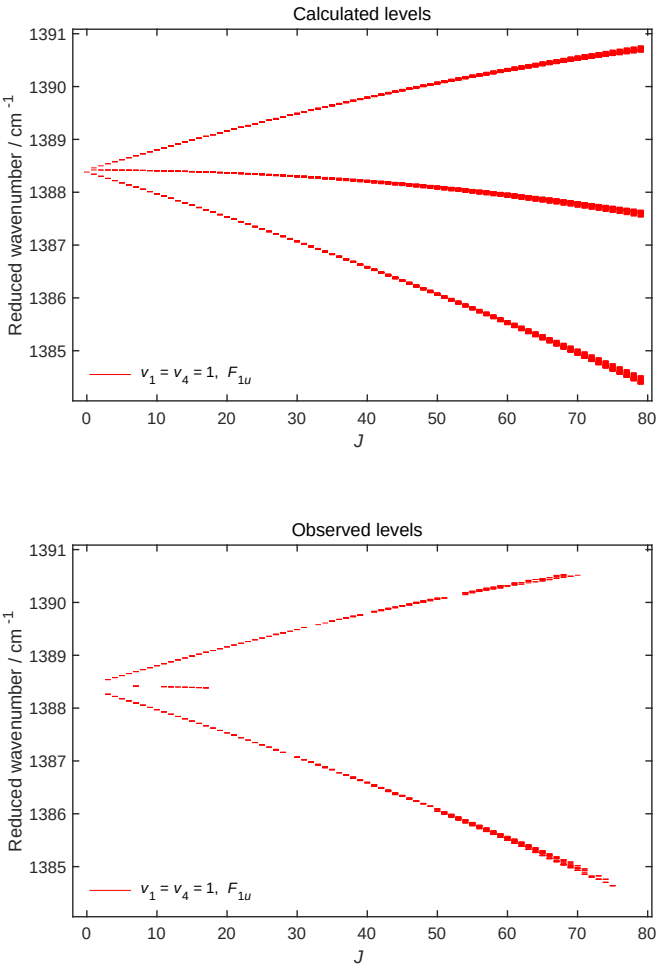

Figure 3: Calculated and observed (*i.e.* reached by assigned transitions) rovibrational energy levels for the $\nu_1 + \nu_4$ combination band of SF_6.

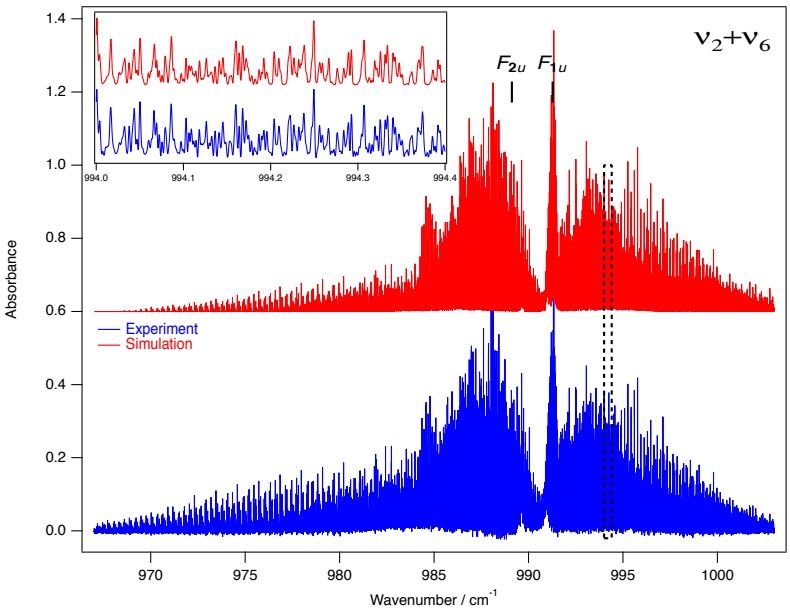

Figure 4: Experimental and simulated spectra for the $\nu_2 + \nu_6$ combination band of SF_6 at 153 K. The insert shows a detail in the R branch. The positions of the two sublevels are also marked.

Table 1, with a root-mean-square deviation of 0.451×10^{-3} cm^{-1}. This is the first detailed study and modeling of this band.

Figure 8 displays the fit residuals for line positions. Figure 9 displays reduced calculated and observed rovibrational energy levels for this band, as in the previous cases. We can see, as mentioned above, that the observed levels only sample the F_{1u} sublevels, but that some faint mixings appear. These are due to couplings with the other sublevels that allowed to fit some of their parameters.

5. SHeCaSDa database update

As explained in section 2.3, because of SF_6's complex vibrational level distribution, we have updated the SHeCaSDa database by using 6 different polyad schemes (see Table 2). Four schemes are dedicated to the $^{32}SF_6$ main isotopo-

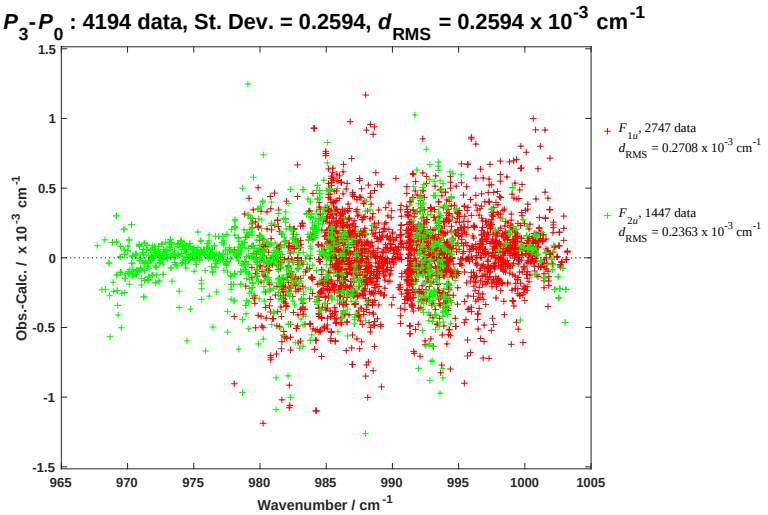

Figure 5: Fit residuals for line positions in the $\nu_2 + \nu_6$ combination band of SF_6.

logue. They correspond to previously defined schemes 1, 2, 4 and 5 (see Section 2.3; scheme 3 is not calculated in the database; see Figures 10 to 12 in the Appendix). The two other simple schemes contain data about the ν_3 fundamental bands of the $^{33}SF_6$, $^{34}SF_6$ and $^{36}SF_6$ isotopologues and about the ν_4 band of the $^{34}SF_6$ isotopologue, respectively (in these schemes, the ground state is P_0 and the fundamental band is P_1). This is a complete refactoring of the previous revision of the base and the old data should be considered as obsolete. It should be noticed that the database only contains lines for which absolute line intensities can be calculated, that are the ν_6, ν_4 and ν_3 cold fundamental bands and some of the associated hot bands; but these calculations result from the energy levels obtained thanks to all the above-described fits.

A total of 491 500 calculated lines have been included in a new version of the database (see Table 3). The calculated data are accessible either through our website at `http://vamdc.icb.cnrs.fr/PHP/shecasda.php` or on the VAMDC

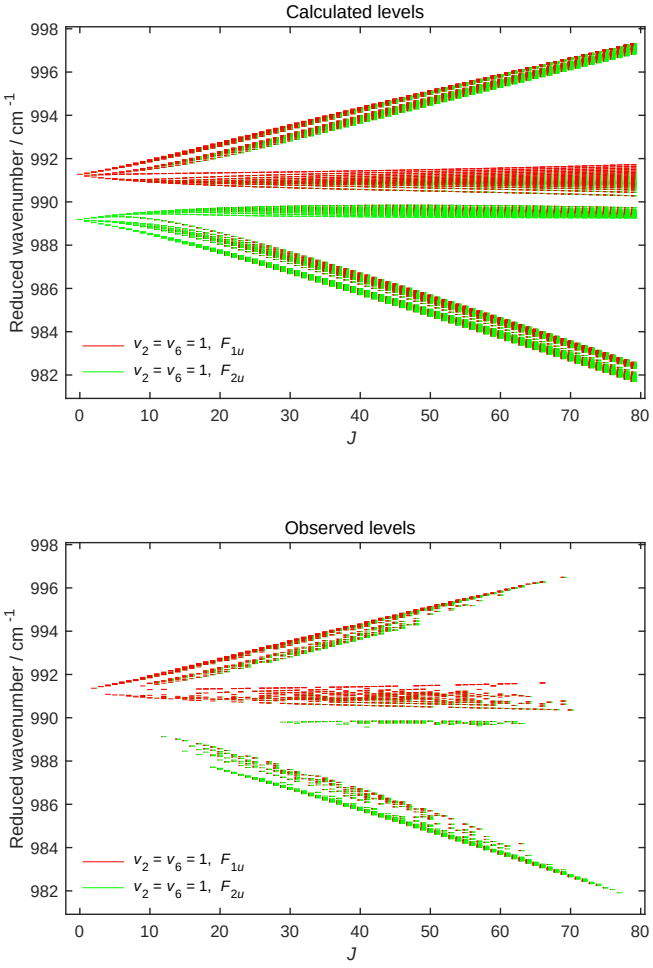

Figure 6: Calculated and observed (*i.e.* reached by assigned transitions) rovibrational energy levels for the $\nu_2 + \nu_6$ combination band of SF_6. Colors show the mixings between the two vibrational sublevels.

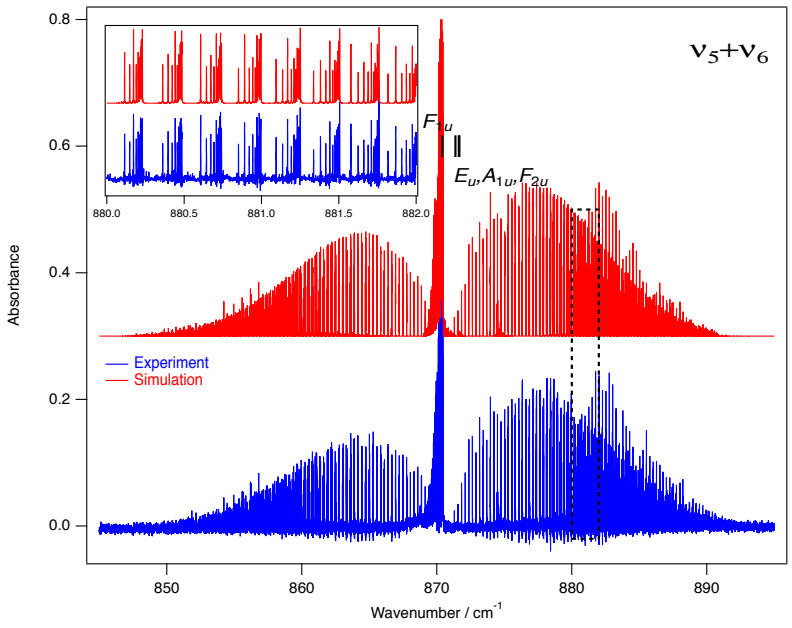

Figure 7: Experimental and simulated spectra for the $\nu_5 + \nu_6$ combination band of SF_6 at 153 K. The insert shows a detail in the R branch. The positions of the four sublevels are also marked.

portal at `https://portal.vamdc.eu/vamdc_portal`. On the first one, it is possible to plot the data and download two sorts of file formats. The line by line list is given following the HITRAN 2004 format[54], while cross section is a simple 2-column flat file.

6. Conclusion and perspectives

This work is a continuation of our previous studies of the rovibrational levels of $^{32}SF_6$ in order to gather information allowing a correct simulation of hot bands in the ν_3 strongly absorbing region. Based on previous global fits, we could model three combination bands: $\nu_2+\nu_6$, which has been strongly improved from the previous studies, while $\nu_1 + \nu_4$ and $\nu_5 + \nu_6$ were analyzed in detail for the first time. These results and those from other recent papers form our group allowed to update the SHeCaSDa database of calculated SF_6 lines. For this

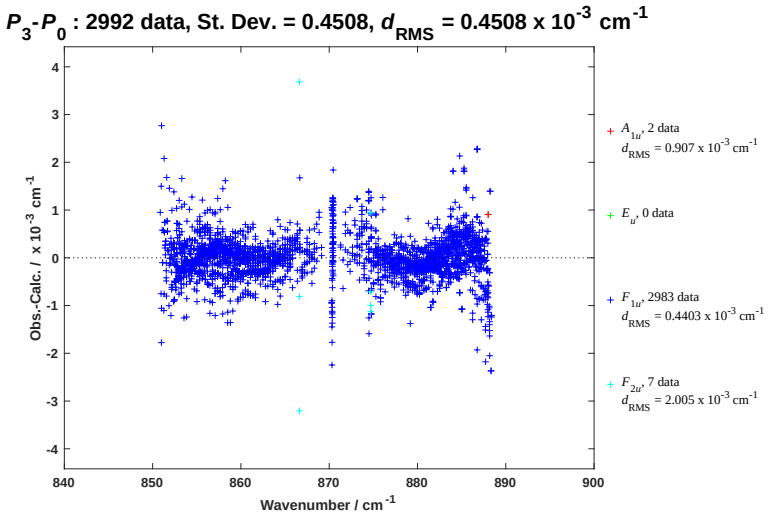

Figure 8: Fit residuals for line positions in the $\nu_5 + \nu_6$ combination band of SF_6.

molecule, some work is still needed, as mentionned in Ref. [46], in order to analyze the $\nu_3 + \nu_6 - \nu_4$ difference band. This one is quite weak and complex, but will lead to the knowledge of the $\nu_3 + \nu_6$ combination level and thus to the calculation of the main hot band in the ν_3 region, namely $\nu_3 + \nu_6 - \nu_6$. Only after that, updates of the HITRAN and GEISA databases for SF_6 would be valuable (knowing also that line-broadening studies would be needed).

Acknowledgements

We thank the LEFE CHAT CNRS program, Ile de France region (program DIM-Analytics) and SOLEIL Management.

Appendix: Polyad schemes

Figures 10 to 13 illustrate the vibrational structure of SF_6 and display the different transitions already analyzed or calculated for this molecule, along with

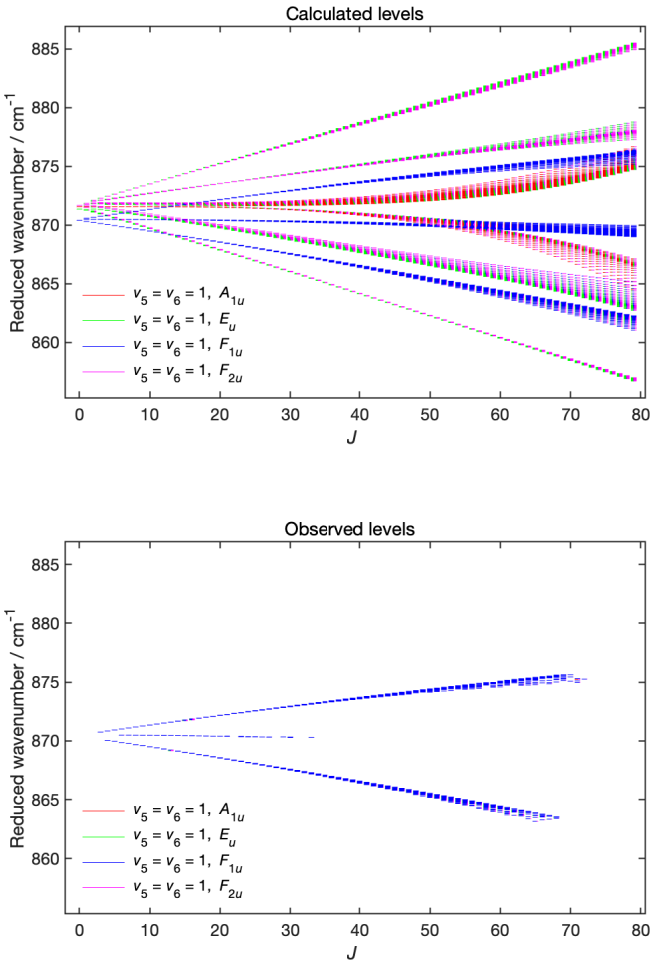

Figure 9: Calculated and observed (*i.e.* reached by assigned transitions) rovibrational energy levels for the $\nu_5 + \nu_6$ combination band of SF_6. Colors show the mixings between the four vibrational sublevels.

Table 2: Number of calculated molecular states in the SHeCaSDa database for the different polyad schemes defined in Section 2.3 and in the Appendix, plus two other simple schemes for the minor isotopologues (P_0 = GS and $P_1 = \nu_3$ or ν_4 in this case). In "Scheme 5", we consider here the $\nu_1 + \nu_4$ band from Figure 13.

Scheme	Levels	Molecular States	Scheme	Levels	Molecular States
Scheme 1 (Figure 10)			Scheme 5 ($\nu_1 + \nu_4$, Figure 13)		
$^{32}SF_6$	P_0	9 501	$^{32}SF_6$	P_1	18 301
	P_1	19 001		P_2	5 901
	P_2	9 501		P_3	17 701
	P_3	28 501	ν_3 of minor isotopologues		
	P_4	66 503	$^{34}SF_6$	P_0	571
	P_5	28 501		P_1	1 620
Scheme 2 (Figure 11)			$^{33}SF_6$	P_0	571
$^{32}SF_6$	P_0	4 251		P_1	1 620
	P_1	12 751	$^{36}SF_6$	P_0	2 734
	P_2	12 751		P_1	82 01
	P_3	38 254	ν_4 of minor isotopologues		
Scheme 4 (Figure 12)			$^{34}SF_6$	P_0	1 354
$^{32}SF_6$	P_0	6 101		P_1	3 920
	P_1	17 701			
	P_3	51 334			

the different polyad schemes that were used. In each case, arrows representing transitions follow the following plot code:

- Continuous lines represent assigned and fitted bands.
- Dashed lines represent calculated bands (typically: a hot band calculated from the difference between two levels that were analyzed on their own).
- Red lines correspond to dipolar absorption.
- Green lines correspond to stimulated Raman transitions.
- Blue lines correspond to two-photo absorption [55].

Table 3: Rovibrational transitions included in the SHeCaSDa database (see Table 2 and Appendix for polyad definitions).

Transitions	Nb. dipolar	Dipolar wavenumber range / cm^{-1}	Dipolar intensity range / $cm^{-1}/(molecule\ cm^{-2})$	Polarisability intensity range / arbitrary unit
Scheme 1 (Figure10)				
$^{32}SF_6$				
$P_1 - P_0$	42 983	600–687		2.0×10^{18}–6.0×10^{20}
$P_2 - P_0$	7 861	773–775		2.0×10^{17}–3.0×10^{21}
$P_4 - P_0$	11 797	770–773		2.0×10^{17}–2.0×10^{20}
$P_3 - P_0$	53 996	935–957	8.0×10^{-24}–1.6×10^{-20}	
$P_4 - P_1$	32 371	932–959	8.0×10^{-24}–8.0×10^{-22}	
$P_5 - P_2$	11 473	937–949	8.0×10^{-24}–3.6×10^{-22}	
Scheme 2 (Figure11)				
$^{32}SF_6$				
$P_2 - P_0$	14 941	593–637	8.0×10^{-24}–1.2×10^{-21}	
$P_3 - P_1$	34 575	593–637	8.0×10^{-24}–2.0×10^{-22}	
$P_1 - P_0$	62 895	320–374	8.0×10^{-29}–4.0×10^{-26}	
Scheme 4 (Figure12)				
$^{32}SF_6$				
$P_1 - P_0$	59 842	475–562		2.0×10^{18}–4.0×10^{20}
$P_3 - P_0$	12 1841	932–964		
Scheme 5 ($\nu_1 + \nu_4$, Figure13)				
$^{32}SF_6$				
$P_3 - P_1$	17 987	772–773		3.0×10^{17}–2.0×10^{20}
$P_3 - P_1$	3 935	599–630	8.0×10^{-24}–2.8×10^{-23}	
ν_3 of minor isotopologues				
$^{34}SF_6$				
$P_1 - P_0$	1 620	928–933	2.0×10^{-22}–1.6×10^{-20}	
$^{33}SF_6$				
$P_1 - P_0$	1 620	937–941	2.0×10^{-22}–1.6×10^{-20}	
$^{36}SF_6$				
$P_1 - P_0$	7 843	908–920	1.2×10^{-21}–1.6×10^{-20}	
ν_4 of minor isotopologues				
$^{34}SF_6$				
$P_1 - P_0$	3 920	600–624	1.6×10^{-23}–1.2×10^{-21}	

- Orange lines on Figure 12 also represent dipolar absorption transitions from Ref. [30]; this color is used to distinguish polyad schemes 3 and 4.

It should be noticed that, in scheme 1 (Figure 10), $2\nu_1$ and $\nu_2 + \nu_3$ are grouped into polyad P_4, while $2\nu_3$ and $\nu_1 + \nu_2 + \nu_3$ are grouped into polyad P_6. This is for convenience and consistency with lower polyads, but, in each case, both bands having opposite parity, there is no interaction between them (no intra-polyad interaction). There is no polyad P_7 nor P_8 in this scheme.

Concerning polyad schemes 5 (Figure 13), used for the study of each combination band of the present work, the polyad definition is given in Section 2.3.

Step 1 – Scheme 1

Simultaneous fit of 12 transitions:

$P_1 - P_0$	$P_3 - P_1$
$P_2 - P_0$	$P_3 - P_2$
$P_3 - P_0$	$P_4 - P_2$
$P_5 - P_0$	$P_6 - P_3$
$P_6 - P_0$	
$P_9 - P_0$	$P_4 - P_1$ and $P_5 - P_2$ are also calculated

to get parameters for:

GS, ν_2 , ν_1 , ν_3 , $2\nu_1$, $\nu_2+\nu_3$, $\nu_1+\nu_3$, $2\nu_3$, $\nu_1+\nu_2+\nu_3$, $3\nu_3$

GS is fixed in steps 3 to 5 to the values obtained here.

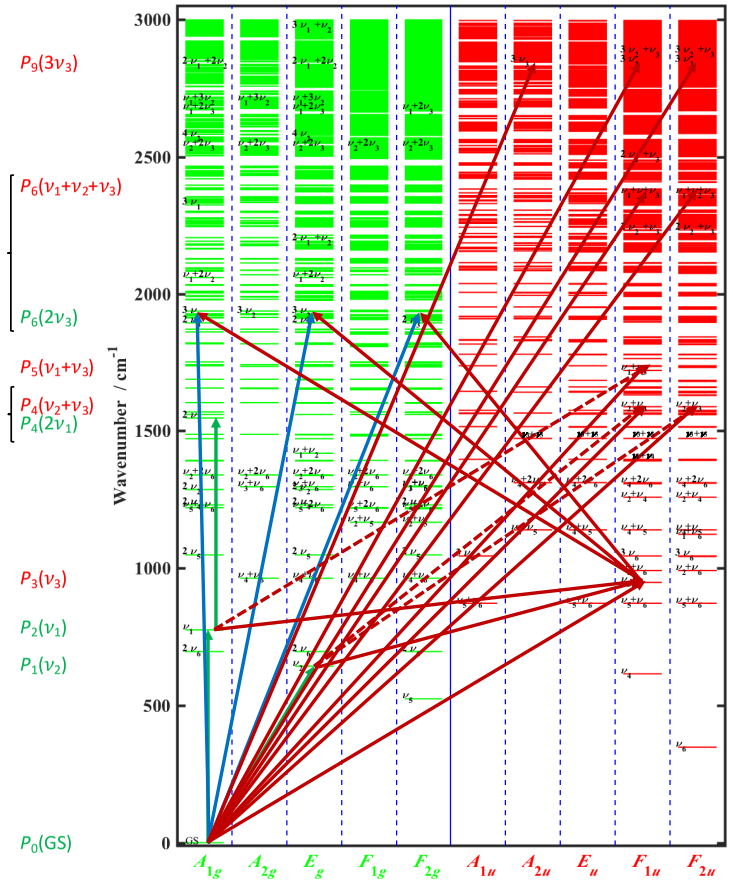

Figure 10: First polyad scheme implying stretching modes ν_1, ν_2 and ν_3. For instance, the ν_3 cold fundamental band constitutes $P_3 - P_0$ transitions in this scheme; $P_5 - P_2$ transitions are $\nu_3 + \nu_1 - \nu_1$ hot band lines.

Step 2 – Scheme 2

Simultaneous fit of 3 transitions:

$P_1 - P_0$
$P_2 - P_0$
$P_3 - P_1$

to get parameters for:

ν_6
ν_4
ν_4+ν_6

which are fixed in steps 3 and 5 to the values obtained here.

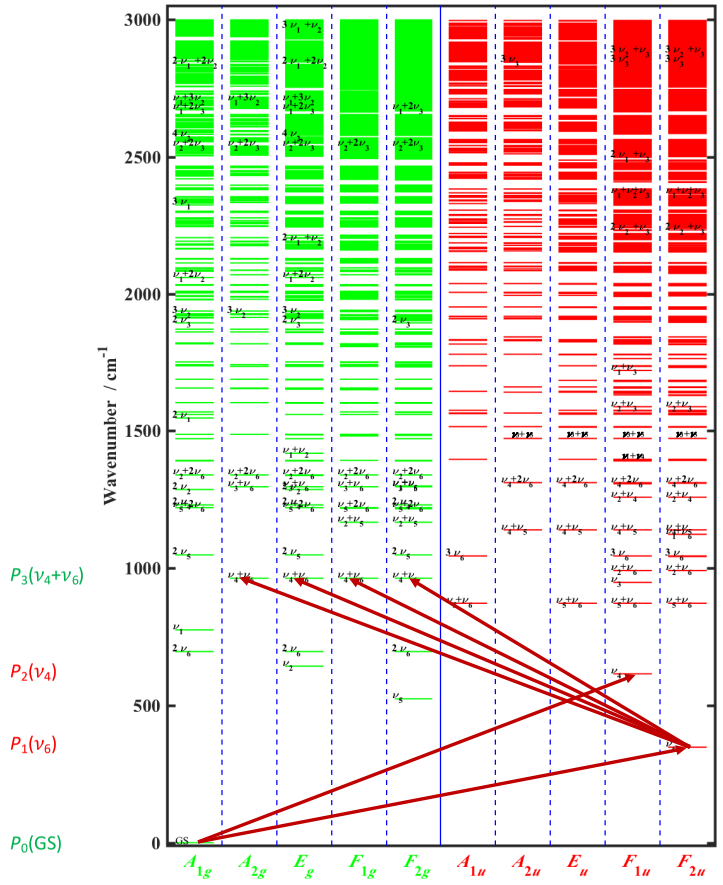

Figure 11: Second polyad scheme implying bending modes ν_4 and ν_5. For instance, the ν_6 and ν_4 cold fundamental bands constitute $P_1 - P_0$ and $P_2 - P_0$ transitions in this scheme, respectively; $P_3 - P_1$ transitions are $\nu_4 + \nu_6 - \nu_6$ hot band lines.

Step 3 – Scheme 3

Fit of 1 transition:

$P_6 - P_1$

to get parameters for:

ν_5, ν_2+ν_4

ν_5 are fixed in steps 4 and 5 to the values obtained here.

Step 4 – Scheme 4

Fit of 1 transition:

ν_3+ν_5–GS

ν_3+ν_5– ν_5 is then calculated.

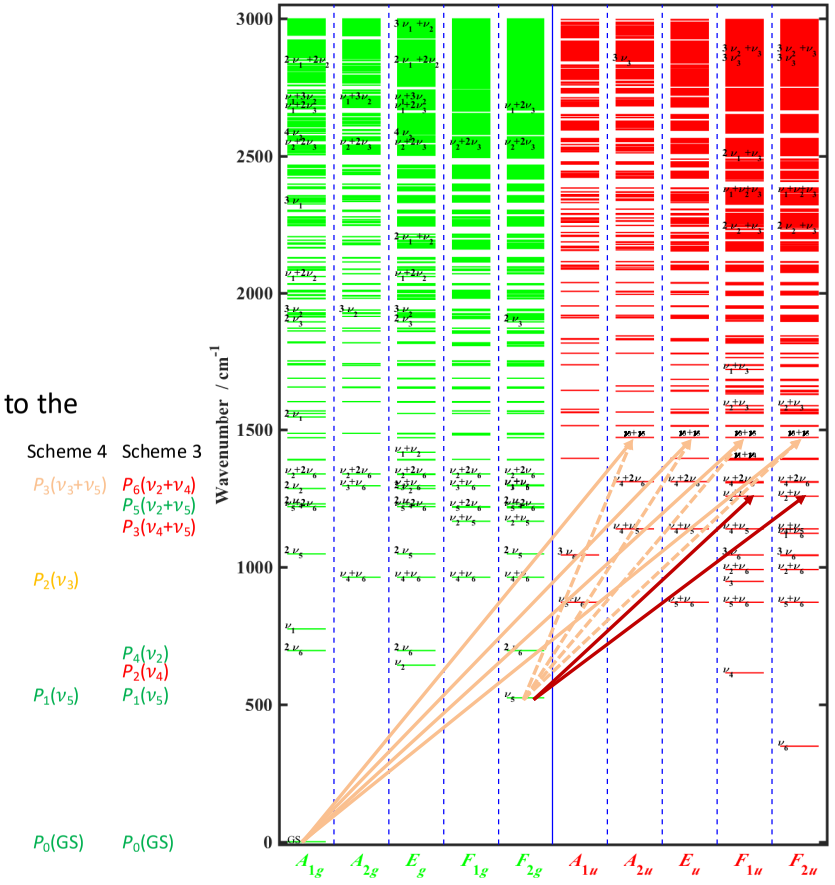

Figure 12: Third and fourth polyad schemes implying bending mode ν_5.

Step 5 – Other schemes

Fit of 3 transitions :

ν_1+ν_4–GS
ν_2+ν_6–GS
ν_5+ν_6–GS

Using previous parameters for ν_1, ν_2, ν_5 and ν_6.

At this stage, they are considered as isolated, with a simple polyad scheme in each case.

The ν_4+ν_1–ν_1 hot band can be calculated.

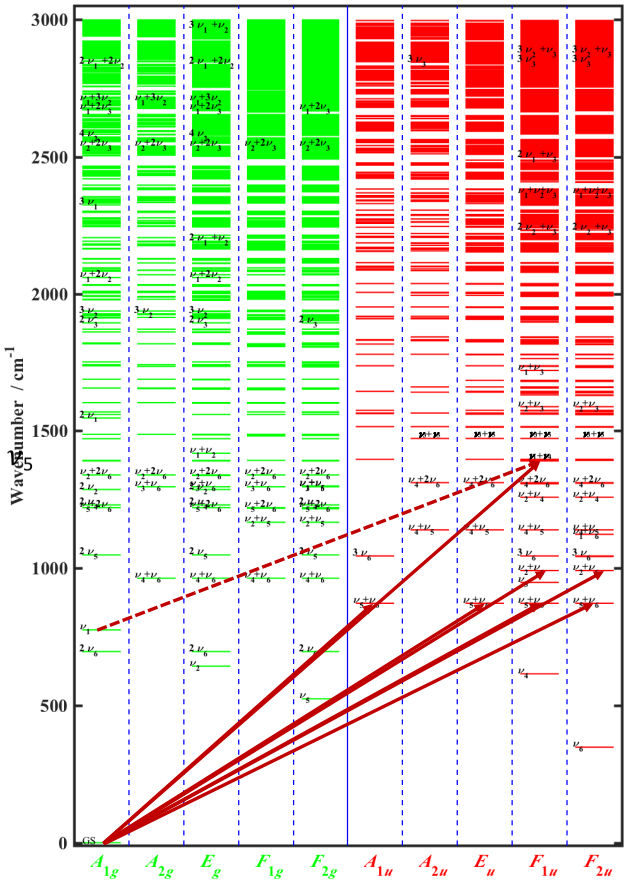

Figure 13: Fifth polyad schemes used for the combination bands fitted in the present work.

References

[1] J. Harnisch, R. Borchers, P. Fabian, M. Maiss, Tropospheric trends for CF_4 and C_2F_6 since 1982 from SF_6 dated stratospheric air, Geophys. Res. Lett. 23 (1996) 1099–1102.

[2] L. Geller, J. Elkins, J. Lobert, A. Clarke, D. Hurst, J. Butler, R. Myers, Tropospheric SF_6 : Observed latitudinal distribution and trends, derived emissions and interhemispheric exchange time, Geophys. Res. Lett. 24 (6) (1997) 675–678.

[3] C. Dervos, P. Vassiliou, Sulphur hexafluoride (SF_6) : Global environmental effects and toxic byproduct formation, Air & Waste Manage. Assoc. 50 (2000) 137–141.

[4] D. T. Ho, P. Schlosser, Atmospheric SF_6 near a large urban area, Geophys. Res. Lett. 27 (11) (2000) 1679–1682.

[5] J. Harnisch, N. Höhne, Comparison of emissions estimates derived from atmospheric measurements with national estimates of HFCs, PFCs and SF_6, Environ. Sci. & Pollut. Res. 9 (5) (2002) 315–320.

[6] C. P. Rinsland, C. Boone, R. Nassar, K. Walker, P. Bernath, E. Mathieu, R. Zander, J. C. McConnell, L. Chiou, Trends of HF, HCl, CCl_2F_2, CCl_3F, $CHClF_2$ (HFC-22), and SF_6 in the lower stratosphere from Atmospheric Chemistry Experiment (ACE and Atmospheric Trace Molecule Spectroscopy (ATMOS) measurements near 30°N latitude, Geophys. Res. Lett. 32 (2005) L16S03–1–5.

[7] D. A. Deeds, M. K. Vollmer, J. T. Kulongoski, B. R. Miller, J. Mühle, C. M. Harth, J. A. Izbicki, D. R. Hilton, R. F. Weiss, Evidence for crustal degassing of CF_4 and SF_6 in Mojave Desert groundwaters, Geochim. et Cosmochim. Acta 72 (2008) 999–1013.

[8] M. J. H. M. Harmsen, D. P. van Vuuren, D. R. Nayak, A. F. Hof, L. Höglund-Isaksson, P. L. Lucas, J. B. Nielsen, P. Smith, E. Stehfest,

Data for long-term marginal abatement cost curves of non-co_2 greenhouse gases, Data in Brief 25 (2019) 104334.

[9] E. Mathieu, R. Zander, M. Gunson, G. Toon, C. Rinsland, P. Demoulin, Evaluation of the lifetime of SF_6 in the Earth's atmosphere, based on ATMOS and Jungfraujoch IR solar observations, in: Atmospheric Spectroscopy Applications 96, Reims, 4–9 Sept. 1996, 1996, pp. 125–128.

[10] E. Manzini, J. Feichter, Simulation of the SF_6 tracer with the middle atmosphere MAECHAM4 model : Aspects of the large-scale transport, J. Geophys. Res. 104 (D24) (1999) 31097–31108.

[11] E. Kjellström, J. Feitcher, G. Hoffman, Transport of SF_6 and $^{14}CO_2$ in the atmospheric general circulation model ECHAM4, Tellus 52B (2000) 1–18.

[12] C. S. Law, A. P. Martin, M. I. Liddicoat, A. J. Watson, K. J. Richards, E. M. S. Woodward, A Lagrangian SF_6 tracer study of an anticyclonic eddy in the North Atlantic : Patch evolution, vertical mixing and nutriment supply to the mixed layer, Deep-Sea Res. II 48 (2001) 705–724.

[13] C. S. Law, A. J. Watson, Determination of persian gulf water transport and oxygen utilisation rates using SF_6 as a novel transient tracer, Geophys. Res. Lett. 28 (5) (2001) 815–818.

[14] H. Yang, D. W. Waugh, C. Orbe, P. K. Patra, P. Jöckel, J.-F. Lamarque, S. Tilmes, D. Kinnison, J. W. Elkins, E. J. Dlugokency, Evaluating simulations of interhemispheric transport: Interhemispheric exchange time versus sf_6 age, Geophys. Res. Lett. 46 (2019) 1113–1120.

[15] V. Boudon, G. Pierre, Rovibrational spectroscopy of sulphur hexafluoride: A review, in: S. G. Pandalai (Ed.), Recent research developments in molecular spectroscopy, Vol. 1, Transworld Research Network, Trivandrum, India, 2002, pp. 25–55.

[16] I. E. Gordon, L. S. Rothman, R. V. C. Hill and, Y. Tan, P. F. Bernath, M. Birk, V. Boudon, A. Campargue, K. V. Chance, B. J. Drouin, J.-M.

Flaud, R. R. Gamache, J. T. Hodges, D. Jacquemart, V. I. Perevalov, A. Perrin, K. P. Shine, M.-A. H. Smith, J. Tennyson, G. C. Toon, H. Tran, V. G. Tyuterev, A. Barbe, A. Csaszar, M. V. Devi, T. Furtenbacher, J. J. Harrison, A. Jolly, T. Johnson, T. Karman, I. Kleiner, A. A. Kyuberis, J. Loos, O. M. Lyulin, S. T. Massie, S. N. Mikhailenko, N. Moazzen-Ahmadi, H. S. P. Müller, O. V. Naumenko, A. V. Nikitin, O. L. Polyansky, M. Rey, M. Rotger, S. Sharpe, K. Sung, E. Starikova, S. A. Tashkun, J. V. Auwera, G. Wagner, J. Wilzewski, P. Wcisło, S. Yu, E. J. Zak, The HITRAN2016 Molecular Spectroscopic Database, J. Quant. Spectrosc. Radiat. Transfer 203 (2017) 3–69.

[17] N. Jacquinet-Husson, R. Armante, N. A. Scott, A. Chedin, L. Crepeau, C. Boutammine, A. Bouhdaoui, C. Crevoisier, V. Capelle, C. Boonne, N. Poulet-Crovisier, A. Barbe, D. C. Benner, V. Boudon, L. R. Brown, J. Buldyreva, A. Campargue, L. H. Coudert, V. M. Devi, M. J. Down, B. J. Drouin, A. Fayt, C. Fittschen, J. M. Flaud, R. R. Gamache, J. J. Harrison, C. Hill, O. Hodnebrog, S. M. Hu, D. Jacquemart, A. Jolly, E. Jimenez, N. N. Lavrentieva, A. W. Liu, L. Lodi, O. M. Lyulin, S. T. Massie, S. Mikhailenko, H. S. P. Mueller, O. V. Naumenko, A. Nikitin, C. J. Nielsen, J. Orphal, V. I. Perevalov, A. Perrin, E. Polovtseva, A. Predoi-Cross, M. Rotger, A. A. Ruth, S. S. Yu, K. Sung, S. A. Tashkun, J. Tennyson, V. I. G. Tyuterev, J. V. Auwera, B. A. Voronin, A. Makie, The 2015 edition of the GEISA spectroscopic database, J. Mol. Spectrosc. 327 (2016) 31–72.

[18] R. McDowell, H. Galbraith, C. Cantrell, N. Nereson, E. Hinkley, The ν_3 q branch of SF_6 at high resolution : Assignments of the levels pumped by $P(16)$ of the CO_2 laser, J. Mol. Spectrosc. 68 (1977) 288–298.

[19] R. McDowell, B. Krohn, Vibrational levels and anharmonicity in SF_6 – I. Anharmonic and potential constants, Spectrochim. Acta. 42A (2/3) (1986) 371–385.

[20] R. McDowell, B. Krohn, H. Flicker, M. C. Vasquez, Vibrational levels and

anharmonicity in SF_6 – I. Vibrational band analysis, Spectrochim. Acta. 42A (2/3) (1986) 351–369.

[21] V. Boudon, M. Hepp, M. Herman, I. Pak, G. Pierre, High-resolution jet-cooled spectroscopy of SF_6 : The $\nu_2 + \nu_6$ combination band of $^{32}SF_6$ and the ν_3 band of the rare isotopomers, J. Mol. Spectrosc. 192 (1998) 359–367.

[22] D. Bermejo, R. Z. Martínez, E. Loubignac, V. Boudon, G. Pierre, Simultaneous analysis of the ν_2 Raman and $\nu_2 + \nu_6$ infrared spectra of the SF_6 molecule, J. Mol. Spectrosc. 201 (2000) 164–171.

[23] V. Boudon, D. Bermejo, First high-resolution Raman spectrum and analysis of the ν_5 bending fundamental of SF_6, J. Mol. Spectrosc. 213 (2002) 139–144.

[24] V. Boudon, J. L. Doménech, D. Bermejo, H. Willner, High-resolution Raman spectroscopy of the ν_1 region and Raman-Raman double resonance spectroscopy of the $2\nu_1 - \nu_1$ band of $^{32}SF_6$ and $^{34}SF_6$. Determination of the equilibrium bond length of sulfur hexafluoride, J. Mol. Spectrosc. 228 (2004) 392–400.

[25] V. Boudon, J. L. Doménech, A. Ramos, D. Bermejo, H. Willner, High-resolution stimulated Raman spectroscopy and analysis of the ν_2, ν_5 and $2\nu_6$ bands of $^{34}SF_6$, Mol. Phys. 104 (16–17) (2006) 2653–2661.

[26] V. Boudon, G. Pierre, H. Bürger, High resolution spectroscopy and analysis of the $\nu 4$ bending region of SF_6 near 615 cm^{-1}, J. Mol. Spectrosc. 205 (2001) 304–311.

[27] V. Boudon, N. Lacome, High-resolution FTIR spectrum and analysis of the $\nu_2 + \nu_4$ combination band of $^{32}SF_6$, J. Mol. Spectrosc. 222 (2003) 291–295.

[28] V. Boudon, P. Asselin, P. Soulard, M. Goubet, T. Huet, R. Georges, O. Pirali, P. Roy., High-resolution spectroscopy and analysis of the $\nu_2 + \nu_3$ combination band of SF_6 in a supersonic jet expansion, Mol. Phys. 111 (2154–2162) (2013).

[29] M. Faye, A. L. Ven, V. Boudon, L. Manceron, P. Asselin, P. Soulard, F. Kwabia Tchana, P. Roy, High-resolution spectroscopy of difference and combination bands of SF_6 to elucidate the $\nu_3 + \nu_1 - \nu_1$ and $\nu_3 + \nu_2 - \nu_2$ hot band structures in the ν_3 region, Mol. Phys. 112 (2014) 2504–2514.

[30] M. Faye, L. Manceron, P. Roy, V. Boudon, M. Loëte, First analysis of the $\nu_3 + \nu_5$ combination band of sf_6 observed at doppler-limited resolution and effective model for the $\nu_3 + \nu_5 - \nu_5$ hot band, J. Mol. Spectrosc. 348 (2018) 37–42.

[31] V. Boudon, L. Manceron, F. Kwabia Tchana, M. Loëte, L. Lago, P. Roy, Resolving the forbidden band of SF_6, Phys. Chem. Chem. Phys. 16 (2014) 1415–1423.

[32] M. Faye, V. Boudon, M. Loëte, P. Roy, L. Manceron, The high overtone and combination levels of SF_6 revisited at doppler-limited resolution: A global effective rovibrational model for highly excited vibrational states, J. Quant. Spectrosc. Radiat. Transfer 190 (2017) 38–47.

[33] M. Faye, L. Manceron, P. Roy, V. Boudon, M. Loëte, First high resolution analysis of the ν_3 band of the $^{36}SF_6$ isotopologue, J. Mol. Spectrosc. 346 (2018) 23–26.

[34] J.-P. Champion, M. Loëte, G. Pierre, Spherical top spectra, in: K. N. Rao, A. Weber (Eds.), Spectroscopy of the Earth's atmosphere and interstellar medium, Academic Press, San Diego, 1992, pp. 339–422.

[35] V. Boudon, J.-P. Champion, T. Gabard, M. Loëte, F. Michelot, G. Pierre, M. Rotger, C. Wenger, M. Rey, Symmetry-adapted tensorial formalism to model rovibrational and rovibronic spectra of molecules pertaining to various point groups, J. Mol. Spectrosc. 228 (2004) 620–634.

[36] V. Boudon, J.-P. Champion, T. Gabard, M. Loëte, M. Rotger, C. Wenger, Spherical top theory and molecular spectra, in: M. Quack, F. Merkt (Eds.),

Handbook of High Resolution Spectroscopy, Vol. 3, John Wiley & Sons, Ltd, Chichester, 2011, Ch. 39, pp. 1437–1460.

[37] M. Rey, V. Boudon, M. Loëte, Tensorial development of the rovibronic Hamiltonian and transition moment operators for octahedral molecules, J. Mol. Struct. 599 (2001) 125–137.

[38] V. Boudon, J.-P. Champion, T. Gabard, G. Pierre, M. Loëte, C. Wenger, Spectroscopic tools for remote sensing of greenhouse gases CH_4, CF_4 and SF_6, Environ. Chem. Lett. 1 (2003) 86–91.

[39] C. Wenger, V. Boudon, M. Rotger, J. P. Sanzharov, J. P. Champion, XTDS and SPVIEW: Graphical tools for the analysis and simulation of high-resolution molecular spectra, Journal of Molecular Spectroscopy 251 (2008) 102–113.

[40] M. L. Dubernet, V. Boudon, J. L. Culhane, M. S. Dimitrijevic, A. Z. Fazliez, C. Joblin, F. Kupka, G. Leto, P. L. Sidaner, P. A. Loboda, H. E. Mason, N. J. Mason, C. Mendoza, G. Mulas, T. J. Millar, L. A. Nuñez, V. I. Perevalov, N. Piskunov, Y. Ralchenko, G. Rixon, L. S. Rothman, E. Roueff, T. A. Ryabchikova, A. Ryabtsev, S. Sahal-Bréchot, B. Schmitt, S. Schlemmer, J. Tennyson, V. G. Tyuterev, N. A. Walton, V. Wakelam, C. J. Zeippen, Virtual atomic and molecular data centre, J. Quant. Spectrosc. Radiat. Transfer 111 (2010) 2151–2159.

[41] Y. A. Ba, C. Wenger, R. Surleau, V. Boudon, M. Rotger, L. Daumont, D. A. Bonhommeau, V. G. Tyuterev, M.-L. Dubernet, MeCaSDa and ECaSDa: Methane and ethene calculated spectroscopic databases for the virtual atomic and molecular data centre, Journal of Quantitative Spectroscopy and Radiative Transfer 130 (2013) 62–68.

[42] M. L. Dubernet, B. K. Antony, Y. A. Ba, Y. L. Babikov, K. Bartschat, V. Boudon, B. J. Braams, H.-K. Chung, F. Daniel, F. Delahaye, G. D. Zanna, J. de Urquijo, A. Domaracka, M. Doronin, B. J. Drouin, M. S. Dimitrijevic, C. P. Endres, E. Quintas-Sanchez, A. Z. Fazliev, S. V. Gagarin,

I. E. Gordon, U. Heiter, C. Hill, D. Jevremovic, C. Joblin, A. Kasprzak, E. Krishnakumar, G. Leto, P. A. Loboda, T. Louge, S. Maclot, B. P. Marinkovic, A. Markwick, T. Marquart, H. E. Mason, N. J. Mason, C. Mendoza, A. A. Mihajlov, T. J. Millar, N. Moreau, G. Mulas, G. Leto, Y. Pakhomov, P. Palmeri, S. Pancheshnyi, V. I. Perevalov, N. Piskunov, J. Postler, P. Gratier, P. Quinet, G. Rixon, Y. Ralchenko, Y.-J. Rhee, L. S. Rothman, E. Roueff, T. Ryabchikova, S. Sahal-Bréchot, P. Scheier, S. Schlemmer, B. Schmitt, E. Stempels, J. Tennyson, V. G. Tyuterev, V. Vujcic, V. Wakelam, N. A. Walton, O. Zatsarinny, C. J. Zeippen, C. M. Zwolf, the VAMDC Consortium, The Virtual Atomic and Molecular Data Centre (VAMDC) consortium for astrophysics, Journal of Physics B 49 (2016) 074003–1–074003–18.

[43] N. Moreau, C. M. Zwolf, Y. A. Ba, C. Richard, V. Boudon, M.-L. Dubernet, The vamdc portal as a major enabled of atomic ans molecular data citation, Galaxies 6 (2018) 105.

[44] H. A. Buckmaster, R. Chatterjee, Y. H. Shing, The application of tensor operators in the analysis of EPR and ENDOR spectra, Phys. Stat. Sol. A 13 (9) (1972) 9–50.

[45] J. H. V. Vleck, On σ-type doubling and electron spin in the spectra of diatomic molecules, Phys. Rev. 33 (1929) 467–506.

[46] M. Faye, V. Boudon, M. Loëte, P. Roy, L. Manceron, Observation and analysis of the SF_6 $\nu_2 + \nu_4 - \nu_5$ band: Improved parameters for the $\nu_5 = 1$ state, J. Mol. Spectrosc. 325 (2016) 35–41.

[47] C. Wenger, V. Boudon, J.-P. Champion, G. Pierre, Highly-Spherical Top Data System (HTDS) software for the spectrum simulation of octahedral XY_6 molecules, J. Quant. Spectrosc. Radiat. Transfer 66 (1) (2000) 1–16.

[48] P. Roy, J.-B. Brubach, M. Rouzières, O. Pirali, F. Kwabia Tchana, L. Manceron, Ailes: La ligne infrarouge et thz sur rayonnement synchrotron soleil, Revue de l'électricité et de l'électronique 2008 (3) (2008) 23–30.

[49] J.-B. Brubach, L. Manceron, M. Rouzières, O. Pirali, D. Balcon, F. Tchana, V. Boudon, M. Tudorie, T. Huet, A. Cuisset, P. Roy, Performance of the AILES THz-infrared beamline on SOLEIL for high resolution spectroscopy, AIP Conference Proceeding 1214 (2010) 81–84.

[50] M. Faye, Signature infrarouge et modélisation pour la télédétection de deux gaz: SF_6 et RuO_4, Th'ese de doctorat (Univ. Paris -Sud and Univ. Paris Saclay) (2017).

[51] F. Kwabia Tchana, F. Willaert, X. Landsheere, J.-M. Flaud, L. Lago, M. Chapuis, C. Herbeaux, P. Roy, L. Manceron, A new, low temperature long-pass cell for mid-infrared to terahertz spectroscopy and synchrotron radiation use, Review of Scientific Instruments 84 (9) (2013) 093101.

[52] S. Chernin, E. Barskaya, Optical multipass matrix systems, Appl. Opt. 30 (1991) 51–58.

[53] R. A. Toth, Transition frequencies and absolute strengths of $H_2{}^{17}O$ and $H_2{}^{18}O$ in the 6.2 μm region, J. Opt. Soc. Am. B 9 (1992) 462–482.

[54] L. S. Rothman, D. Jacquemart, A. Barbe, D. C. Benner, M. Birk, L. R. Brown, M. R. Carleer, C. C. Jr., K. Chance, L. H. Coudert, V. Dana, V. M. Devi, J.-M. Flaud, R. R. Gamache, A. Goldman, J.-M. Hartmann, K. W. Jucks, A. G. Maki, J.-Y. Mandin, S. T. Massie, J. Orphal, A. Perrin, C. P. Rinsland, M. A. H. Smith, J. Tennyson, R. N. Tolechov, R. A. Toth, J. Vander Auwera, P. Varanasi, G. Wagner, The HITRAN 2004 molecular spectroscopic database, J. Quant. Spectrosc. Radiat. Transfer 96 (2005) 139–204.

[55] F. Herlemont, M. Khelkhal, J. Legrand, G. Pierre, Doppler-free two-photon spectrum of SF_6 for metrological purposes, Optics Letters. 23 (12) (1997) 957–959.